AGU PUBLICATIONS

JGR

Journal of Geophysical Research: Atmospheres

RESEARCH ARTICLE
10.1002/2016JD026424

Why was the arid and semiarid northwest China getting wetter in the recent decades?

Dongdong Peng[1,2] and **Tianjun Zhou**[1,2,3]

[1]LASG, Institute of Atmospheric Physics, Chinese Academy of Sciences, Beijing, China, [2]College of Earth Science, University of Chinese Academy of Sciences, Beijing, China, [3]Jiangsu Collaborative Innovation Center for Climate Change, Nanjing, China

Key Points:
- The contribution of increased specific humidity is the dominant factor for the wetting trend
- The increasing specific humidity is associated with the enhanced evaporation which is favored by increased downward longwave radiation
- The anomalous ascending motion induced by southward displacement of Asian subtropical westerly jet also contributes to the wetting trend

Correspondence to:
T. Zhou,
zhoutj@lasg.iap.ac.cn

Citation:
Peng, D., and T. Zhou (2017), Why was the arid and semiarid northwest China getting wetter in the recent decades?, *J. Geophys. Res. Atmos.*, *122*, doi:10.1002/2016JD026424.

Received 2 JAN 2017
Accepted 1 JUL 2017
Accepted article online 6 JUL 2017

Abstract The arid and semiarid northwest China has experienced a significant wetting trend in summer during 1961–2010, but the reasons remain ambiguous. In this study, moisture budget analysis is employed to quantify the contributions of different factors to the wetting trend. The results show that more than 50% of the increasing precipitation is balanced by the increased evaporation. The convergence of moisture flux (the sum of horizontal moisture advection and wind convergence terms) has a significant positive contribution to the wetting trend. The increased net surface radiation, which is contributed by the increased downward longwave radiation, supplies more energy to favor the evaporation process of vaporization. The moisture flux convergence is further separated into thermodynamic component in association with changes in specific humidity and dynamic component due to changes in atmospheric circulation. The thermodynamic contribution to the wetting trend is induced by the increased specific humidity which is associated with enhanced evaporation. The dynamic contribution is dominated by an anomalous cyclone over central Asia. The anomalous cyclone is related with intensified horizontal vorticity advection which is associated with a significant southward displacement of Asian subtropical westerly jet. The results indicate that the changes of evaporation against the background of global warming deserve more attention in projecting the climate change in arid and semiarid regions.

1. Introduction

Northwest China (NW) (35–50°N, 74–105°E) is located at the inner land of the Eurasian continent and lies in the shadow of the Tibetan Plateau. NW is a region that has considerable land-atmosphere interaction; the scarce water vapor and climatological descent motion is favorable for NW being a vast arid and semiarid region in Asia, with an annual total precipitation less than 200 mm [*Wu and Qian*, 1996; *Qian et al*., 1998; *Qian et al*., 2001b; *Koster et al*., 2004]. The precipitation amount of NW is concentrated in summer and varies from year to year, which has significant effects on the ecological environment and social development as well as lives of people [*Qian et al*., 2001a; *Ren et al*., 2005; *Chen and Huang*, 2012]. Understanding the physical processes responsible for summer precipitation changes over NW is of great scientific and societal importance.

What is the origin of water vapor transport supplying the rainfall in NW? For the long-term mean, the water vapor in Atlantic Ocean, Arctic ocean, Black Sea, and Caspian Sea is transported into NW following the prevailing westerly [*Li et al*., 2008; *Ren et al*., 2016]. The glacial meltwater and river runoff also supply the moisture in arid and semiarid NW [*Shi et al*., 2007; *Chen et al*., 2013]. The interannual variation of the precipitation in NW are affected by many factors including the subtropical westerly [*Feng et al*., 2004; *Li et al*., 2008], Jet Position Index [*Zhao et al*., 2014b], South Asian High [*Wei et al*., 2017], Western Pacific Subtropical High [*Wu and Qian*, 1996; *Qian et al*., 2001b], and the dynamic and thermodynamic effects of Tibetan Plateau [*Wu and Qian*, 1996; *Qian et al*., 1998; *Qian et al*., 2001a, 2001b]. Remotely, the circumglobal teleconnection pattern, which is induced by the latent heating of Indian summer monsoon, also influences the precipitation in NW [*Ding and Wang*, 2005; *Ding et al*., 2011; *Chen and Huang*, 2012; *Huang et al*., 2015].

Observations show that the precipitation has experienced a wetting trend during the past half century in the arid and semiarid NW and is mainly contributed by the increasing trend of convective precipitation in boreal summer [*Song and Zhang*, 2003; *Ren et al*., 2005; *Shi et al*., 2007; *Chen and Dai*, 2009; *Li et al*., 2016; *Han et al*., 2016]. Against the background of global warming, the precipitation has changed a lot from global to regional scale [*Intergovernmental Panel on Climate Change* (*IPCC*), 2013]. The "richer-get-richer" mechanism, namely, the rainfall increases in climatological convergence regions and decreases in climatological

subsidence regions, explain well the tropical precipitation anomalies [*Chou and Neelin*, 2004; *Held and Soden*, 2006; *Chou et al*., 2009]. However, the changes of precipitation in arid land do not simply follow the mechanism [*Greve et al*., 2014]. Many mechanisms are proposed to explain the wetting trend in NW, including more heavy precipitation associated with global warming [*Jiang et al*., 2013; *Han et al*., 2016], teleconnections with north hemispheric vortex [*Chen and Dai*, 2009] and South Asian summer monsoon [*Zhao et al*., 2014a], the enhancement of convective instability [*Zhou and Huang*, 2010], impacts of west Pacific subtropical high and North America subtropical high on the water vapor transport [*Li et al*., 2016], and also the increased local evaporation [*Ren et al*., 2016]. Nonetheless, the physical mechanism of the wetting trend remains inconclusive. The statistical correlations between precipitation over western China and the west Pacific subtropical high and the North Atlantic subtropical high presented by *Li et al*. [2016] lack physical explanation. The local evaporation is hypothesized to have a contribution [*Ren et al*., 2016], but more evidences are needed. In this study, we aim to investigate the following questions by diagnosing the water vapor budget: First, what are the contributions of different water vapor budget terms to the wetting trends of precipitation? In particular, how about the contributions of thermodynamic term change associated with specific humidity and dynamical terms change associated with circulation? Second, what are the mechanisms responsible for the changes of water vapor budget? To achieve this objective, a quantitative estimation of contributions from different factors to the wetting trend over NW is needed. To achieve these goals, a moisture budget analysis based on reanalysis data, which has been demonstrated to be helpful in understanding global or regional precipitation changes (*Trenberth and Guillemot* [1995], *Feng and Zhou* [2012], *Lin et al*. [2014], *Ma and Zhou* [2015], and *Huang et al*. [2015], among many others), is conducted along with analysis of the underlying mechanisms. We show evidences that the wetting trend is dominated by increased specific humidity which is associated with enhanced evaporation in arid and semiarid NW.

The remainder of this paper is organized as follows: The data sets and analysis methods are introduced in section 2. In section 3, we first evaluate the quality of JRA55, then analyze the wetting trend using moisture budget analysis and discuss the responsible mechanisms. Finally, the main results are concluded in section 4.

2. Data and Methods

2.1. Data Description

The data sets used in the present study include the following:

1. *Monthly mean precipitation at 756 stations from China's National Meteorological Information Center* (NMIC, http://cdc.nmic.cn/home.do). Following *Zhai et al*. [1999], the stations with missing values exceeding 9 years during 1961–2010 were deleted. After that, 625 station records were retained. As has been revealed by *Ma et al*. [2015], there are less than 5% stations with significant discontinuities, such as the Xiangjiang Zhaosu County and Yanyuan County, suggesting the good quality of the stations' data sets. Thus, the study of regional averaged long-term precipitation changing characteristics using the stations' data sets, as is illustrated in previous studies [*Qian et al*., 2007; *Lu et al*., 2014], is reliable.
2. *A gridded monthly precipitation with the resolution of 0.25 latitude by 0.25 longitude over China* (hereafter CN05.1) [*Wu and Gao*, 2013]. The CN05.1 data are derived from precipitation data of more than 2000 stations in China using the software of ANUSPLIN developed by the Australian National University. Owing to the relative few stations, the uncertainty of precipitation in western China is larger than that in eastern China, with the largest uncertainty over the north part of the Tibetan Plateau and Taklimakan desert [*Wu and Gao*, 2013; *Ji and Kang*, 2015; *Zhou et al*., 2015].
3. *The Japanese 55 year Reanalysis conducted by the Japan Meteorology Agency's (JMA) operational data assimilation and numerical weather model* [*Kobayashi et al*., 2015]. The model used to produce JRA55 is the TL319 spectral resolution version of the JMA global spectral model. JRA55 is at the resolution of 1.25 latitude by 1.25 longitude and covers the period from 1958 to present. The monthly mean variables are employed in this study, e.g., precipitation, evaporation, radiation fluxes, near-surface variables, and vertically integrated moisture. To calculate the moisture budget components, 6-hourly specific humidity, surface pressure, meridional and zonal wind, and pressure velocity are used. All the data were downloaded from the website of *JMA* [2013].

2.2. Method Description

2.2.1. Definition of Northwest China

In China Climate Bulletin for 2013 [*CMA*, 2014], China is divided into several subregions, and northwest China (NW: 35–50°N, 74–105°E) is employed in this study. There are 99 stations in NW among the 625 stations; hence, we named those stations' data 99NW. Note that the wetting trend are mainly located at western northwest China (WNW: 35–50°N, 74–96°E) [*C. Zhao et al.*, 2014; *Li et al.*, 2016]. Thus, we focused on the core region WNW.

2.2.2. Moisture Budget Analysis

To understand the potential mechanism of wetting trend in WNW, a method of moisture budget analysis, which has been commonly used in many studies [*Trenberth and Guillemot*, 1995; *Seager et al.*, 2010; *Chou and Lan*, 2012; *Chou et al.*, 2013], was employed in this study. At the p level coordination, the equation of continuity can be expressed as

$$\nabla_{\boldsymbol{h}}\cdot\overrightarrow{\boldsymbol{V_h}} + \partial_p\omega = 0 \tag{1}$$

Here $\nabla_{\boldsymbol{h}}$ denotes the horizontal differential operator. $\overrightarrow{\boldsymbol{V_h}}$ and ω are the horizontal vector wind and pressure velocity, respectively. The subscript p represents vertical direction at the p level coordination.

The moisture budget equation is

$$\boldsymbol{P} = \boldsymbol{E} - \partial_t < q > - < \nabla_{\boldsymbol{h}}\cdot\overrightarrow{\boldsymbol{V_h}}\, q > - < \partial_p q\omega > + \delta \tag{2}$$

where $\boldsymbol{P}$ and $\boldsymbol{E}$ denote precipitation and evaporation, respectively. q is the specific humidity. Triangle parenthesis indicates a vertical integration from surface to tropopause. On a seasonal scale, the time derivative of vertical integral of specific humidity $\partial_t < q >$ is smaller and neglected. The residual term δ refers to the surface processes linking with topography and model bias [*Trenberth and Guillemot*, 1995; *Seager et al.*, 2010; *Ma and Zhou*, 2015]. At the surface and tropopause, $\omega \approx 0$, leading to $<\partial_p q\omega>$ = 0. The term $- < \nabla_{\boldsymbol{h}}\cdot\overrightarrow{\boldsymbol{V_h}}\, q >$ is the moisture flux convergence. The vertical integral of equation (1) can be transformed as $- < \omega\ \partial_p q >= - < q\ \nabla_{\boldsymbol{h}}\cdot\overrightarrow{\boldsymbol{V_h}} >$, meaning that the vertical moisture advection ($- <\omega\partial_p q>$) is equal to the horizontal wind convergence $\left(- < q\ \nabla_{\boldsymbol{h}}\cdot\overrightarrow{\boldsymbol{V_h}} >\right)$. Therefore, equation (2) can be written as

$$\boldsymbol{P} = \boldsymbol{E} - < \overrightarrow{\boldsymbol{V_h}}\nabla_{\boldsymbol{h}}\cdot q > - < \omega\partial_p q > + \delta \tag{3}$$

Based on equation (3), the changes of precipitation can be decomposed as

$$\boldsymbol{P}' = E' - < \overrightarrow{\boldsymbol{V_h}}\nabla_{\boldsymbol{h}}\cdot q >' - < \omega\partial_p q >' + \delta' \tag{4}$$

Here the primes indicate departures from the long-term mean. The pressure velocity ω, zonal wind u, and specific humidity q are separated as the long-term mean and corresponding departure, namely, $\omega = \overline{\omega} + \omega'$, $u = \overline{u} + u'$, and $q = \overline{q} + q'$. Following *Chou and Lan* [2012], the term $- <\omega\partial_p q>'$ can be further divided as

$$- < \omega\partial_p q >' = - < \overline{\omega}\partial_p q' > - < \omega'\partial_p\overline{q} > - < \omega'\partial_p q' > \tag{5}$$

Here $- < \overline{\omega}\ \partial_p q' >$ only involves changes of specific humidity q, while $- < \omega'\ \partial_p\overline{q} >$ only involves changes of pressure velocity ω. On the large scale, $- < \overline{\omega}\ \partial_p q' >$ and $- < \omega'\ \partial_p\overline{q} >$ are mainly contributed by changes of temperature and atmospheric circulation, respectively. Hence, $- < \overline{\omega}\ \partial_p q' >$ and $- < \omega'\ \partial_p\overline{q} >$ are considered as the thermodynamic and dynamic contributions, respectively. The nonlinear term $- <\omega'\partial_p q'>$ is associated with changes of both q and ω. Likewise, the changes of zonal moisture advection term $- <u\partial_x q>'$ are further decomposed as

$$- < u\partial_x q >' = - < \overline{u}\partial_x q' > - < u'\partial_x\overline{q} > - < u'\partial_x q' > \tag{6}$$

The right terms of equation (6) are the thermodynamic, dynamic, and nonlinear components of zonal moisture advection term, respectively [*Seager et al.*, 2010].

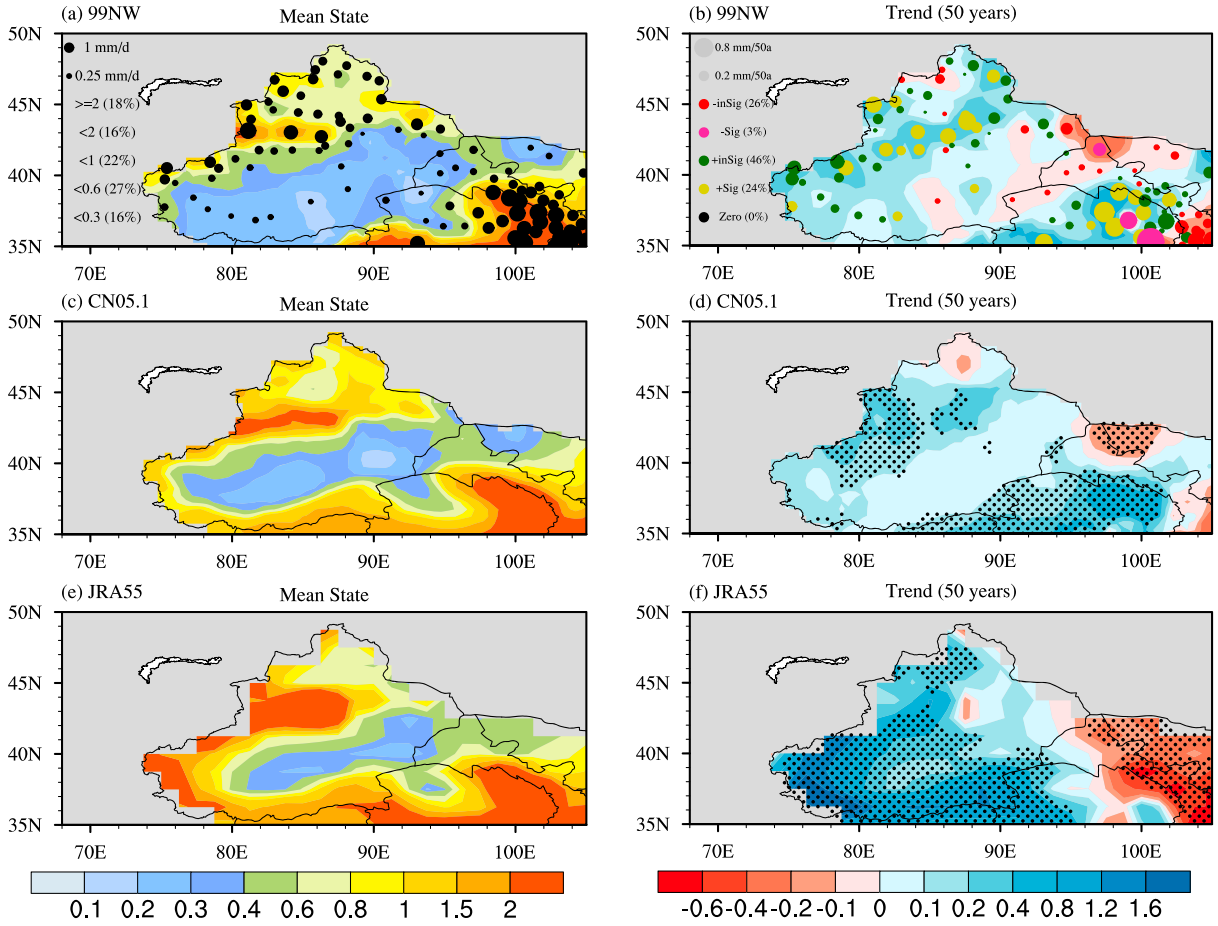

Figure 1. Distribution of June-July-August (JJA) mean (a, c, e; shading, mm d^{-1}) and trend (b, d, f; shading, mm d^{-1} 50 yr^{-1}) of precipitation over northwest China (NW). The results from 99 stations in NW (hereafter, 99NW) (Figures 1a and 1b), CN05.1 (Figures 1c and 1d), and JRA55 (Figures 1e and 1f). Black dots in Figure 1a (Figure 1b) indicate the mean state (long-term trend) of station data, and the size is proportional to the magnitude of precipitation intensity (trend), corresponding to the strings of top left corner. Shading in Figures 1a, 1c, and 1e (Figures 1b, 1d, and 1f) indicates the climatology (long-term trend) of precipitation. Black dots in Figures 1b, 1d, and 1f indicate that the trends were statistically significant at the 10% level. The core region with wetting trend is located in the western northwest China (WNW: 35°–50°N, 74°–96°E).

2.2.3. Asian Subtropical Jet Position Index

In this study, we employed the definition of Asian subtropical jet position index (JPI) in *Hong and Lu* [2016], which is defined as the first leading empirical orthogonal function of 200 hPa zonal wind over the domain 20 to 60°N, 0°–150°E. The JPI is useful in measuring the meridional displacement of Asian subtropical westerly jet (ASWJ).

3. Results

3.1. Evaluation of JRA55 Reanalysis

3.1.1. Precipitation Over NW

We first examine the quality of precipitation derived from the JRA55 data. The geographic distributions of June-July-August (JJA) mean precipitation in NW during 1961–2010 are shown in Figures 1a, 1c, and 1e. The results derived from original stations and grid interpolating are given in Figure 1a, with the percentages of stations from different precipitation intensity in the top left corner. Only 18% of the stations have JJA mean precipitation exceeding 2 mm d^{-1} and are mainly located at the eastern NW. More than half (65%) of the stations show that JJA mean precipitation is less than 1 mm d^{-1}, with the driest stations located over vast areas of western and southern NW. The climatological JJA mean precipitation in NW declines from east to west and from north to south. These characteristics of JJA mean precipitation are also evident in CN05.1

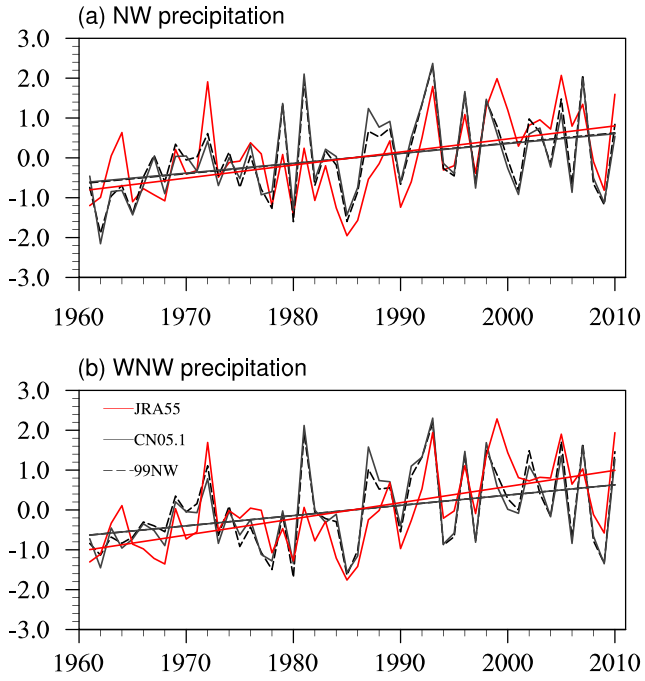

Figure 2. The standardized time series of summer mean precipitation averaged over (a) NW and (b) WNW, and corresponding linear trends. All the trends are statistically significant at 10% level. Black dash lines indicate the 99NW, grey solid lines indicate the CN05.1, and red solid lines indicate the JRA55.

(Figure 1c). The precipitation derived from JRA55 resembles both CN05.1 and 99NW in spatial pattern (Figure 1e), although JRA55 tends to overestimate the amount of summer mean precipitation with respect to observations.

In the past decades, the NW has witnessed a wetting trend, as evidenced by the positive trends in most stations of 99NW, with 70 stations showing positive trends and 27 stations showing negative trends. (Figure 1b). Following the increase of JJA mean precipitation over Qinghai and Xinjiang (35–50°N, 74–96°E), a decreasing trend is seen in the eastern and northeastern NW. Both observations indicate that the JJA mean precipitation increases over almost the whole NW, except for some parts of eastern NW which show negative trends and Taklimakan desert which has sparse stations. The differences of precipitation trends between CN05.1 and NW99 are mainly located at the Taklimakan desert. The observed increasing trends decline from west to east in northern NW from east to west in southern NW, as reported in previous studies [*Chen and Dai*, 2009; *C. Zhao et al.*, 2014; *Li et al.*, 2016]. The spatial patterns of increasing trends can also be found in JRA55. Comparing with the observations, there are some discrepancies in JRA55, such as the overestimated magnitude of precipitation trends and the increasing trends in Taklimakan desert. The observed trends of precipitation are generally well captured by JRA55 (Figure 1f), although the precipitation product of JRA55 is also strongly affected by the deficiencies of its assimilating model.

3.1.2. Time Series of Area-Averaged Precipitation Over NW

To examine the skill of JRA55 in simulating area-averaged characteristics over NW, the normalized time series of JJA mean precipitation are shown in Figure 2. The observational climate mean value of area-averaged precipitation over NW is 0.713 mm d^{-1} for 99NW and 1.004 mm d^{-1} for CN05.1 (Table 1). JRA55 overestimates the climate mean value (1.323 mm d^{-1}) with respect to observations. The interannual standard deviation of JRA55 (0.222 mm d^{-1}) is also higher than that of 99NW (0.099 mm d^{-1}) and CN05.1 (0.103 mm d^{-1}). The time series of 99NW are highly correlated with CN05.1 (with correlation coefficient *r* equal to 0.980); both observations indicate that the JJA precipitation has increased significantly (at 10% confidence level) at a rate of 0.025 mm d^{-1} $decade^{-1}$. The evolution of area-averaged summer precipitation in JRA55 resembles observations, with correlation coefficient *r* equal to 0.711 for 99NW and 0.626 for CN05.1 data; both are statistically significant at the 10% level. The area-averaged precipitation increases in NW derived from the JRA55 is

Table 1. Values of the Area-Averaged Precipitation Over NW[a]

	Mean (mm d^{-1})	Stddev (mm d^{-1})	Trend (mm d^{-1} $decade^{-1}$)	Cor1 (99NW)	Cor2 (CN05.1)
99NW	0.713	0.099	0.025	1.000	
CN05	1.004	0.103	0.025	0.978	
JRA55	1.323	0.222	0.072	0.711	0.626

[a]Mean: the climatology. Stddev: standard deviation. Cor1: correlation with 99NW data. Cor2: correlation with CN05.1 data. All the trends and correlation coefficients are statistically significant at the 10% level.

Table 2. Same as Table 1 But for the Precipitation Over WNW[a]

	Mean (mm d^{-1})	Stddev (mm d^{-1})	Trend (mm d^{-1} $decade^{-1}$)	Cor1 (99NW)	Cor2 (CN05.1)
99NW	0.554	0.106	0.027	1.000	
CN05	0.872	0.107	0.027	0.980	
JRA55	1.285	0.277	0.111	0.736	0.685

[a]All the trends and correlation coefficients are statistically significant at the 10% level.

0.072 mm d^{-1} $decade^{-1}$, which is significant at 10% level. The increasing summer mean precipitation in NW are dominated by changes in WNW (Table 2).

3.2. Spatial Patterns of Moisture Flux

Analysis of water vapor transport is of great help to understand the increasing trend of precipitation. Figure 3a displays the vertically integrated JJA mean moisture flux. The climatological precipitation in NW is dominated by the prevailing westerly which brings abundant moisture from moisture-divergent Eurasia to NW. There are four strong moisture flux divergence centers located in Aral Sea, Black Sea, Caspian Sea, and Mediterranean Sea. There are two channels for water vapor transport to NW: The first is the prevailing westerly which transports moisture directly to NW north of 43°N. The second is the channel from the east flank of the Iranian plateau.

To reveal the anomalous water vapor transport responsible for the rainfall changes, the standardized area-averaged precipitation is regressed on moisture flux (Figure 3b). Two anomalous anticyclones are evident over Europe and Mongolia, while central Asia sees an anomalous cyclone. The regressions pattern closely

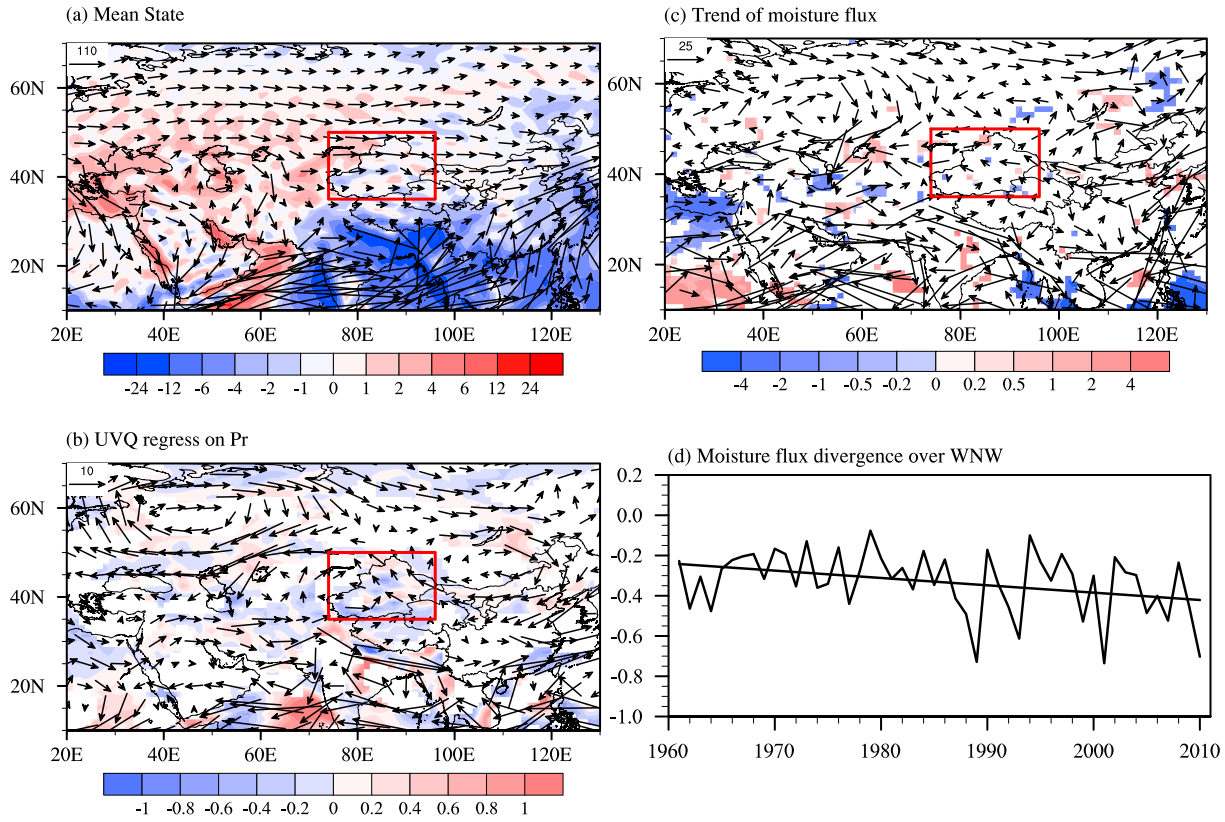

Figure 3. (a) Vertically integrated summer mean water vapor flux during 1961–2010. Vectors indicate the magnitude of moisture flux (kg m^{-1} s^{-1}), and shadings indicate the corresponding divergence (10^{-4} kg m^{-2} s^{-1}). (b) Regression of vertically integrated moisture flux on normalized area-averaged precipitation. Only the regions with changes of zonal or meridional moisture flux statistically significant at the 10% level are shown. (c) The trend of vertically integrated moisture flux (vectors: kg m^{-1} s^{-1} 50 yr^{-1}) and the corresponding divergence (shading: 10^{-4} kg m^{-2} s^{-1} 50 yr^{-1}). Only the regions with changes of moisture flux divergence statistically significant at the 10% level are shown. (d) The area-weighted regional averaged moisture flux divergence over WNW and the corresponding linear trend. The trend is statistically significant at the 10% level. Red box indicates the core region WNW.

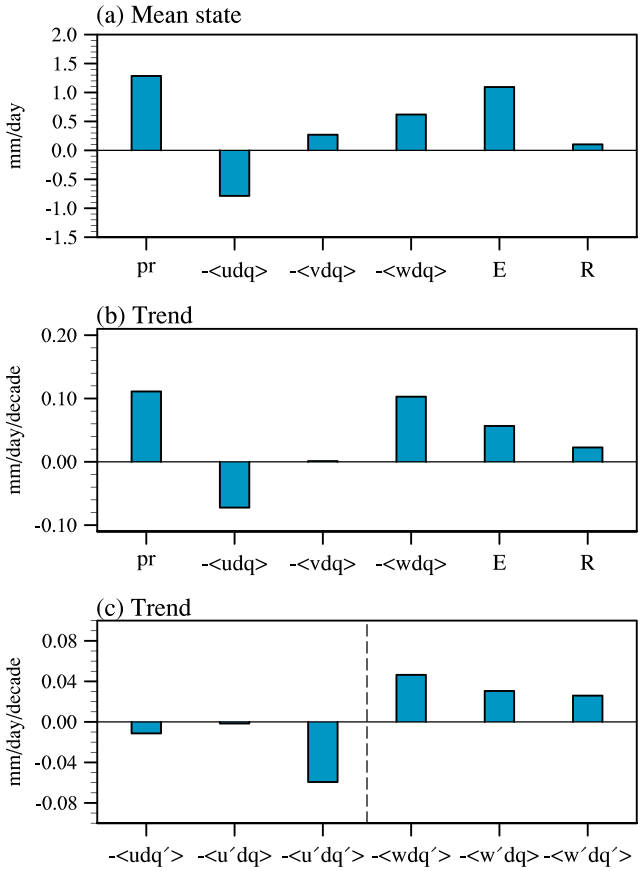

Figure 4. The regional area-averaged moisture budget components in WNW. (a) The climatology and (b and c) the long-term trends. The zonal advection term $-<udq>$ (wind convergence term $-<wdq>$) is broken into thermodynamic term $-<udq'>(-<wdq'>)$, dynamic term $-<u'dq>(-<wdq'>)$, and nonlinear term $-<u'dq'>(-<w'dq'>)$. The units are mm d^{-1} for Figure 4a and mm d^{-1} $decade^{-1}$ for Figures 4b and 4c. Trends of pr (precipitation), *E* (evaporation), $-<udq>$, $-<wdq>$, $-<wdq'>$, and $-<wdq>$ are statistically significant at the 10% level.

resembles the long-term trend for moisture flux in Figure 3c. The anomalous anticyclone over Mongolia and the cyclone over central Asia result in moisture flux divergence over eastern NW and convergence over WNW (which is statistically significant at 5% level, as is shown in Figure 3d.), finally leading to the long-term trend of precipitation in Figure 1f. The anomalous cyclone over central Asia are also favorable for the transport of moisture to the WNW. To the south of Tibetan Plateau, there is an anomalous anticyclone associated with large divergent moisture flux over the Indian subcontinent.

In summary, the increasing moisture flux in WNW is mainly contributed by the decreasing outflow from the eastern boundary and the increasing inflow from the southern boundary.

3.3. Moisture Budget Analysis

The variability of evaporation in JRA55 has been evaluated by *Su et al.* [2015]. The evaporation in JRA55 has a high performance in capturing the observed variability in arid and semiarid China (especially at the interdecadal timescale), although it, as well as Japanese 25 year Reanalysis, has some inaccuracies over eastern China when focusing on the interannual variation [*Liu et al.*, 2014; *Su et al.*, 2015].

We further reveal the physics behind the wetting NW by conducting moisture budget analysis. The area-averaged moisture budget components of WNW precipitation are shown in Figure 4. The climatological magnitude of precipitation is nearly equal to that of evaporation, indicating the importance of land-atmosphere interaction over NW. Due to the negative contribution of zonal advection, the moisture flux convergence (the sum of vertical moisture advection and horizontal moisture advections) contributes a little to the climatological precipitation over NW.

The results derived from moisture budget analysis for the long-term trend is shown in Figure 4b. Both wind convergence term and evaporation over WNW have significant upward trend. More than 50% of the increasing precipitation is balanced by the enhanced evaporation. The zonal advection term shows significant downward trend, while contribution of meridional moisture advection is not evident. The sum of increased wind convergence term and decreased zonal advection term, i.e., the moisture flux convergence, shows a significant increasing trend.

It should be noted that while the water vapor budget diagnosis helps reveal the consistent changes of precipitation and evaporation, it cannot identity the cause-and-effect relationship between them. Previous studies show evidences that the glacial retreat has a significant increasing trend over NW during the past 50 years [*Yao et al.*, 2004; *Lu et al.*, 2005; *Shi et al.*, 2007; *Shangguan et al.*, 2009; *A. H. Wang et al.*, 2011]. Meanwhile, the winter-spring snow shows a significant increasing trend during 1961–2010 [*Sun et al.*, 2010; *Li*, 2013]. The increased glacial meltwater has moistened the land surface over NW, leading to a

significant moistening trend of soil moisture [*P. Wang et al*., 2011] and an increasing trend of river runoff over here [*Lu et al*., 2005; *Shi et al*., 2007]. Although the consistent changes of precipitation and evaporation do not mean a cause-and-effect relationship, the evidences presented above indicate an enhanced contribution of local evaporation to precipitation, through either direct effect or feedback.

Based on equations (5) and (6), the moisture flux convergence term is separated into thermodynamic component, dynamic component, and nonlinear components of zonal and vertical moisture advection terms (Figure 4c). The negative trend of zonal moisture advection term mainly results from the nonlinear component. For the wind convergence term, however, the thermodynamic component is the largest contributor to the wetting trend, followed by dynamic component and nonlinear component. The sum of zonal and vertical nonlinear contributions is negative and small. The dynamic and thermodynamic magnitudes of zonal moisture advection are far less than that of wind convergence term. In summary, the increasing trend of precipitation minus evaporation is dominated by thermodynamic component, followed by dynamic component of the wind convergence term.

The spatial patterns of long-term trend for moisture budget components are shown in Figure 5. Apart from northwest Xinjiang (43–46°N, 82–87°E), evaporation enhances over the whole WNW, with the largest trend over southeast Xinjiang (Figure 5a). The zonal moisture advection term has negative and positive trends over Xinjiang and western Qinghai, respectively (Figure 5b). Due to the canceling effect with positive and negative trends over northern and southern WNW, respectively, the meridional moisture advection term as a whole contributes a little to the wetting trend (Figure 5c). As to the wind convergence term, approximately all the regions over south WNW have significant positive trends (Figure 5d). The spatial patterns of thermodynamic component match well with that of the wind convergence term in southern WNW, confirming that the contribution of wind convergence term largely results from the thermodynamic term. With regard to the spatial patterns of dynamic component, the upward trends are mainly over southwestern WNW. Hence, the contributions of thermodynamic and dynamic components of wind convergence to the increasing precipitation are mainly over southern and southwestern WNW, respectively.

3.4. Mechanisms Responsible for the Increasing Precipitation

As discussed above, changes of precipitation are associated with changes of evaporation, and the increasing trend of precipitation minus evaporation is dominated by thermodynamic component, followed by dynamic component. Therefore, the corresponding mechanisms are examined.

3.4.1. Evaporation

Evaporation is the process by which liquid water is converted to water vapor (i.e., vaporization) and removed from the evaporating surface (i.e., vapor removal). Vaporization and vapor removal, the two key processes, are strongly affected by several near-surface meteorological parameters including air temperature, relative humidity, wind speed, and net surface radiation [*Allen et al*., 1998; *Chattopadhyay and Hulme*, 1997; *Burn and Hesch*, 2007; *Brutsaert*, 2006; *Lorenz et al*., 2010]. Therefore, the correlations between area-averaged evaporation and the four meteorological variables in WNW are presented (Figure 6a). All the four near-surface variables show significant (at the 5% confidence level) correlation with the evaporation, with the correlation coefficient equal to 0.347 for air temperature, 0.728 for relative humidity, 0.915 for net surface radiation, and −0.349 for wind speed. According to the Dalton formulation, evaporation can be simplified as $E \propto f(W) \times (e_{\mathrm{surf}} - \mathrm{RH} \times e_{\mathrm{air}})$, where W is the near-surface wind speed, e_{surf} is the surface saturated vapor pressure, e_{air} is the near-surface air-saturated vapor pressure, and RH is the relative humidity of near-surface air. The increasing relative humidity is the result of enhanced evaporation and can reduce the evaporation demand (vapor pressure deficit), thus restraining the increasing rate of evaporation [*Chattopadhyay and Hulme*, 1997; *Allen et al*., 1998]. During the past half century, the surface wind speed shows significant decreasing trend (Figure 8e) and thus has a negative correlation with the evaporation. Therefore, the increasing near-surface air temperature and net surface radiation favor the process of evaporation. The correlation coefficient between evaporation and net surface radiation is largest, suggesting that changes in net surface radiation is the most important factor. Net surface radiation can provide energy for the process of vaporization and thus favors the process of evaporation. The higher the net surface radiation is, the higher rate of evaporation would be.

Net surface radiation is the sum of upward shortwave radiation (USW), downward shortwave radiation (DSW), upward longwave radiation (ULW), and downward longwave radiation (DLW). Note that a positive value

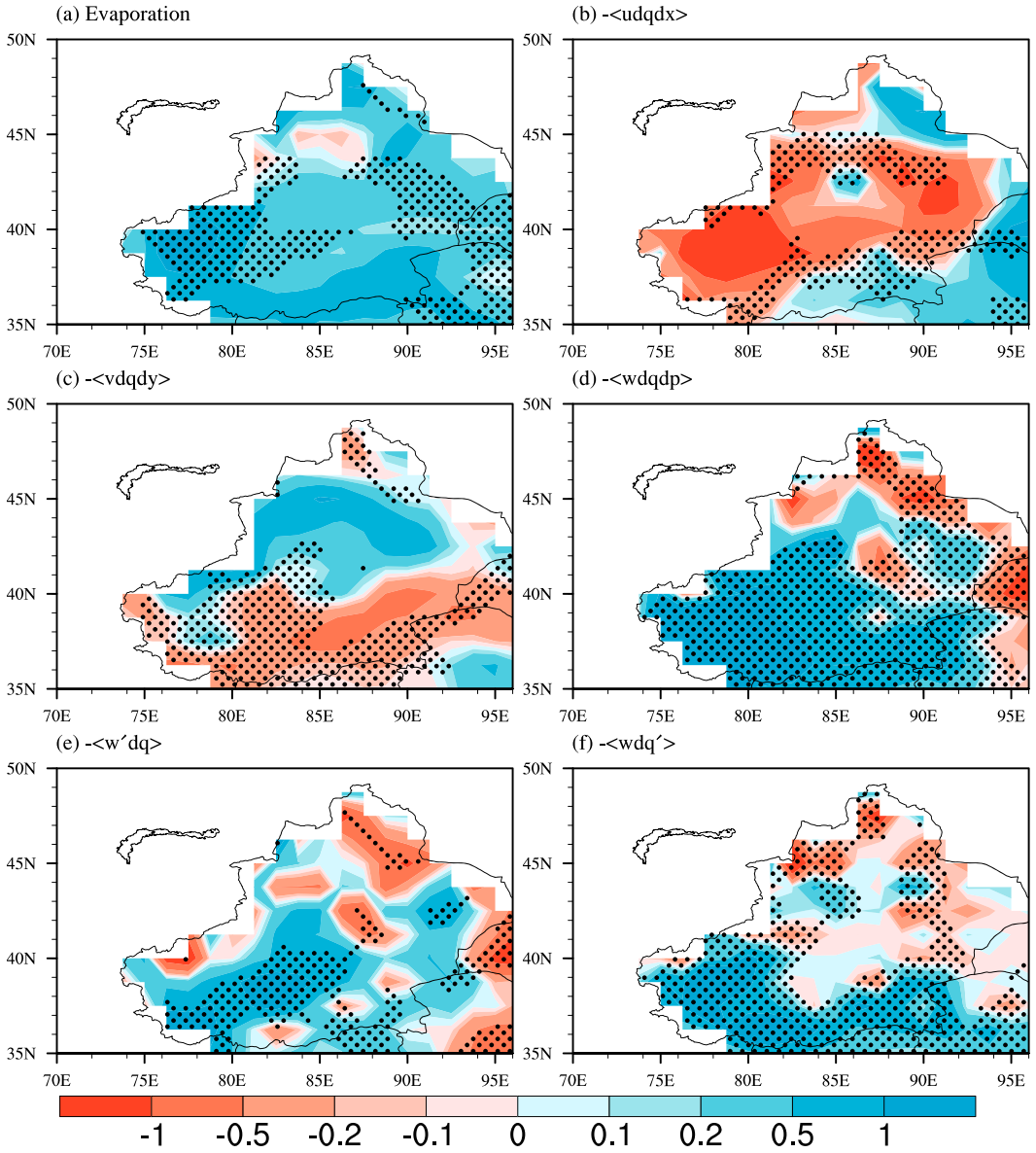

Figure 5. The spatial patterns of linear trends of moisture budget components in JJA during 1961–2010. (a) Evaporation, (b) zonal moisture advection term, (c) meridional moisture advection term, (d) wind convergence term, (e) dynamic components, and (f) thermodynamic components. The units are mm d^{-1} 50 yr^{-1}. Black dots indicate that the trends are statistically significant at the 10% level.

means the direction is downward. The positive trend of net radiation is mainly contributed by that of downward longwave radiation (Figure 6b). Both DSW and USW have decreased significantly during 1961–2010, and the magnitude of the former is larger. The contribution of net shortwave radiation, which is the sum of DLW and USW, is negative, thus decreasing the net surface radiation. DSW, USW, and DLW are broken into the components associated with clear sky and cloud (all-sky minus clear sky), respectively (Figure 6c). The decreased DSW and USW are mainly owing to the effect of cloud radiation, while the increased DLW largely originated from the components of clear sky.

The spatial patterns of radiative components are given in Figure 7. The spatial patterns of net surface radiation resemble that of evaporation, with the largest positive trend over southwest WNW and negative trend over northwest Xinjiang (Figure 7a), confirming the dominant contribution of net surface radiation in increasing evaporation. ULW declines and increases in western and eastern WNW, respectively, with a negative center over southwest Xinjiang. The changes of ULW are associated with changes of surface ground temperature

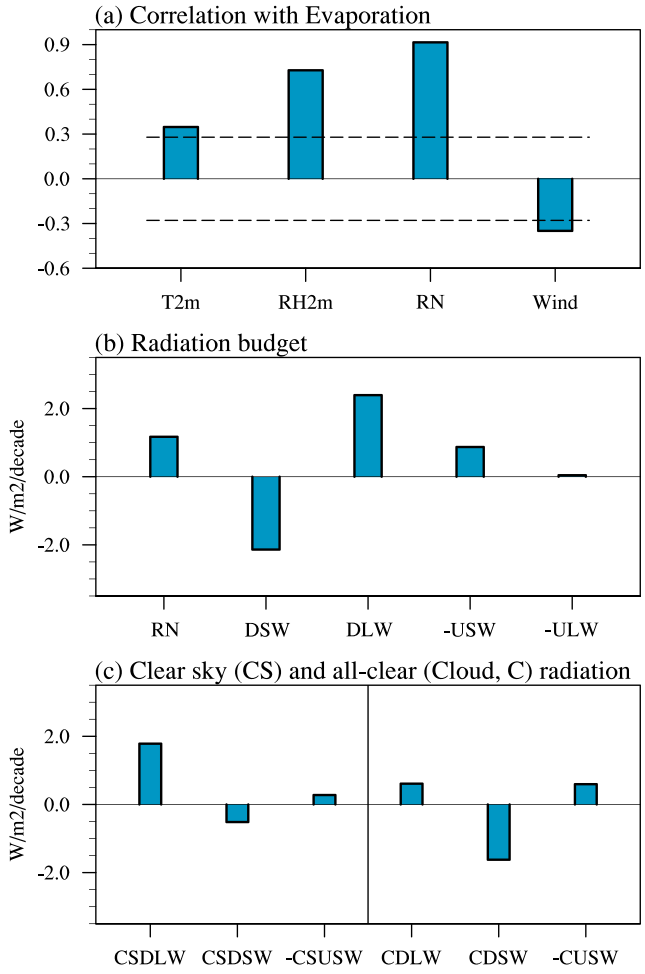

Figure 6. (a) The correlation coefficients between evaporation and near-surface (2 m) air temperature (T2m), relative humidity (RH2m), net radiation (RN), and surface wind speed (Wind). Dash lines indicate that the correlation coefficient is statistically significant at the 5% level. (b) Trend of the radiation variables, namely, RN, downward shortwave radiation (DSW), downward longwave radiation (DLW), upward shortwave radiation (USW), and upward longwave radiation (ULW). (c) Same as Figure 6b, but for clear-sky and all-sky minus clear-sky (all-clear) components of DLW, DSW, and USW, namely, CSDLW, CSDSW, CSUSW, CDLW, CDSW, and CUSW. All the upward radiation variables multiply by -1 to measure the relative contribution of different radiation to RN. Units: W m^{-2} decade^{-1}.

(figure not shown).The location of large center of ULW corresponds to that of net surface radiation, suggesting that the contribution of ULW is mainly located at southwestern Xinjiang. The spatial patterns of DLW match very well with that of net surface radiation, further confirming that the increasing DLW induced by warming atmosphere ($F = \varepsilon\delta T^4$; ε, δ, F, and $T$are the emissivity, Stefan constant, irradiation, and temperature, respectively.) is dominant for the increasing net surface radiation. The effect of cloud radiation has great impact on the shortwave radiation rather than longwave radiation in NW. Due to the increased cloudiness (Figure 8f), DSW shows significant negative trends over the whole WNW. The USW also decreases over WNW and largely results from the cloud components of USW concentrating in southwestern WNW.

In summary, the increased DLW, as determined by warming atmosphere, is the main cause for the increasing net surface radiation.

3.4.2. Thermodynamic Component of Wind Convergence

The contribution of thermodynamic component involves changes in specific humidity against the fixed circulation. In WNW, the thermodynamic contribution to the increasing precipitation is derived from the upward trend of vertically integrated precipitable water (Figure 8a). A large center of positive trend is located over southwest Xinjiang, corresponding to the large center in Figure 5f. On a large scale, the increasing specific humidity is almost entirely contributed by the atmospheric warming under fixed relative humidity [*Seager et al.*, 2010]. On the regional scale of land area, however, the changes of relative humidity cannot be neglected. Since large moisture is concentrated at low level, the changes of near-surface air temperature, specific humidity, and relative humidity are examined. The near-surface specific humidity increases over nearly the whole WNW, with three large centers located over western, southern, and northeastern WNW, respectively (Figure 8d). Likewise, there are three large centers in the near-surface relative humidity, corresponding to the positions in Figure 8d, indicating the importance of changes in specific humidity to changes in relative humidity. However, the positions of three warming centers over southern, northern, and southeastern WNW, respectively, correspond to three low centers of specific humidity and relative humidity. As the increasing rate of specific humidity is larger than that of the air temperature, the relative humidity becomes higher (Clausius Clapeyron relationship $\delta\mathrm{RH} = \frac{\delta e}{e_s} - \frac{L}{R_v T^2}\mathrm{RH}\ \delta T$; RHis the relative humidity, $T$is the temperature, $L$is the latent heat of vaporization, e_s is the saturated vapor pressure, and R_v is the ideal gas constant). Given the significant increasing glacier meltwater and

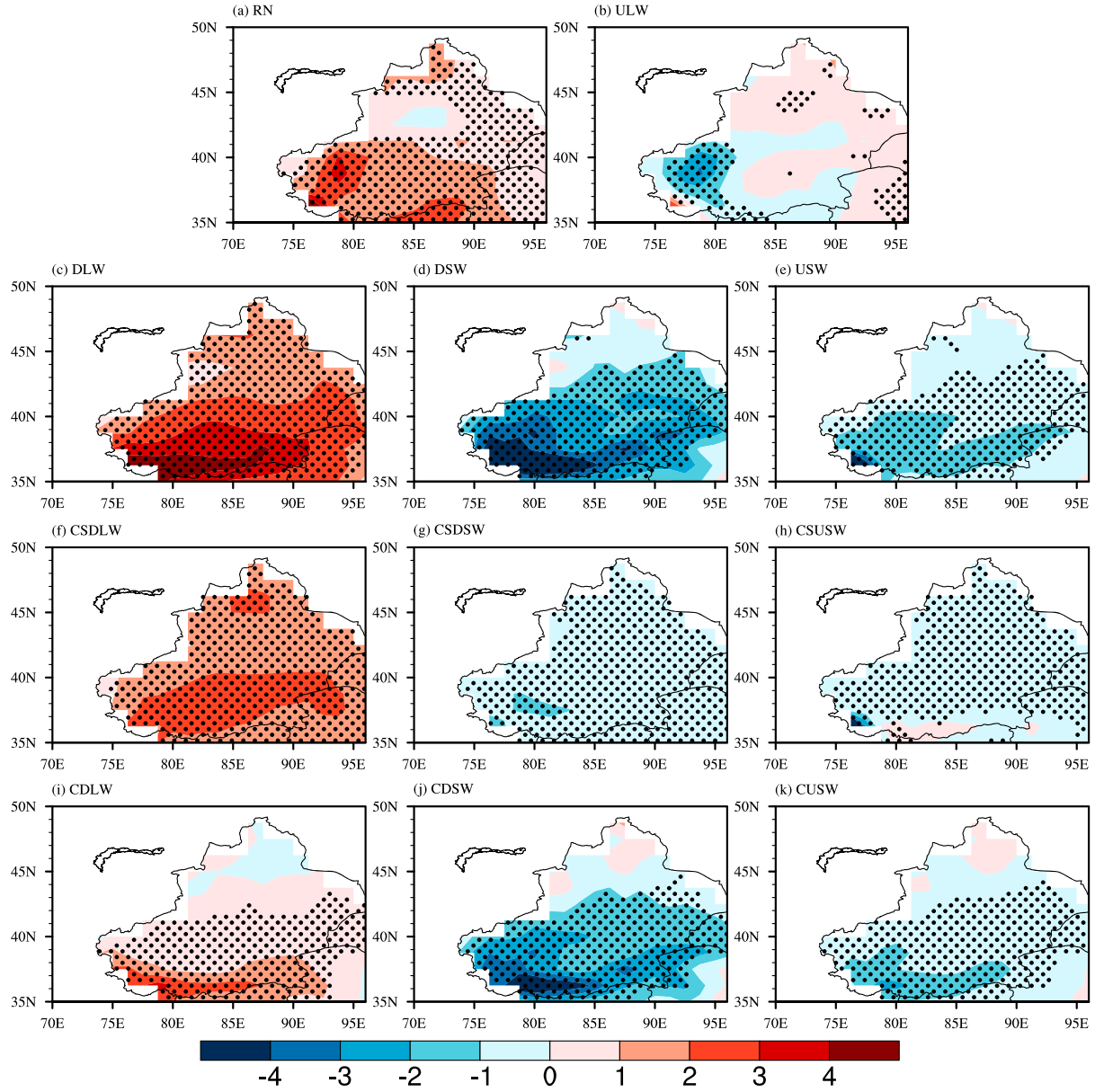

Figure 7. The spatial patterns of linear trends of radiation components in JJA derived from JRA55 during 1961–2010. (a) RN, (b) ULW, (c) DLW, (d) DSW, (e) USW, (f) CSDLW, (g) CSDSW, (h) CSUSW, (i) CDLW, (j) CDSW, and (k) CUSW. Units: W m^{-2} $decade^{-1}$.

winter-to-spring snow during the past 50 years, the increasing specific humidity is mainly associated with the enhanced evaporation.

In summary, the increasing specific humidity, arising from the enhancement of evaporation, is the main cause for the thermodynamic contribution.

3.4.3. Dynamic Component of Wind Convergence

The contribution of dynamic component involves changes in atmospheric circulations under fixed specific humidity. The dynamic contribution to the wetting trend in NW is linked with the anomalous cyclone over central Asia. The JPI index, which is defined as the first leading empirical orthogonal function of zonal wind at 200 hPa over Asia, represents the meridional displacement of ASWJ. During 1961–2010, the ASWJ has a significant southward movement, which is at 10% confidence level (Figures 9a and 9b). The time series of JPI is significantly correlated with WNW precipitation at 10% level (r equals to 0.440 for observations and 0.330 for JRA55, respectively). The JPI time series is regressed on the vorticity advection (defined as wind

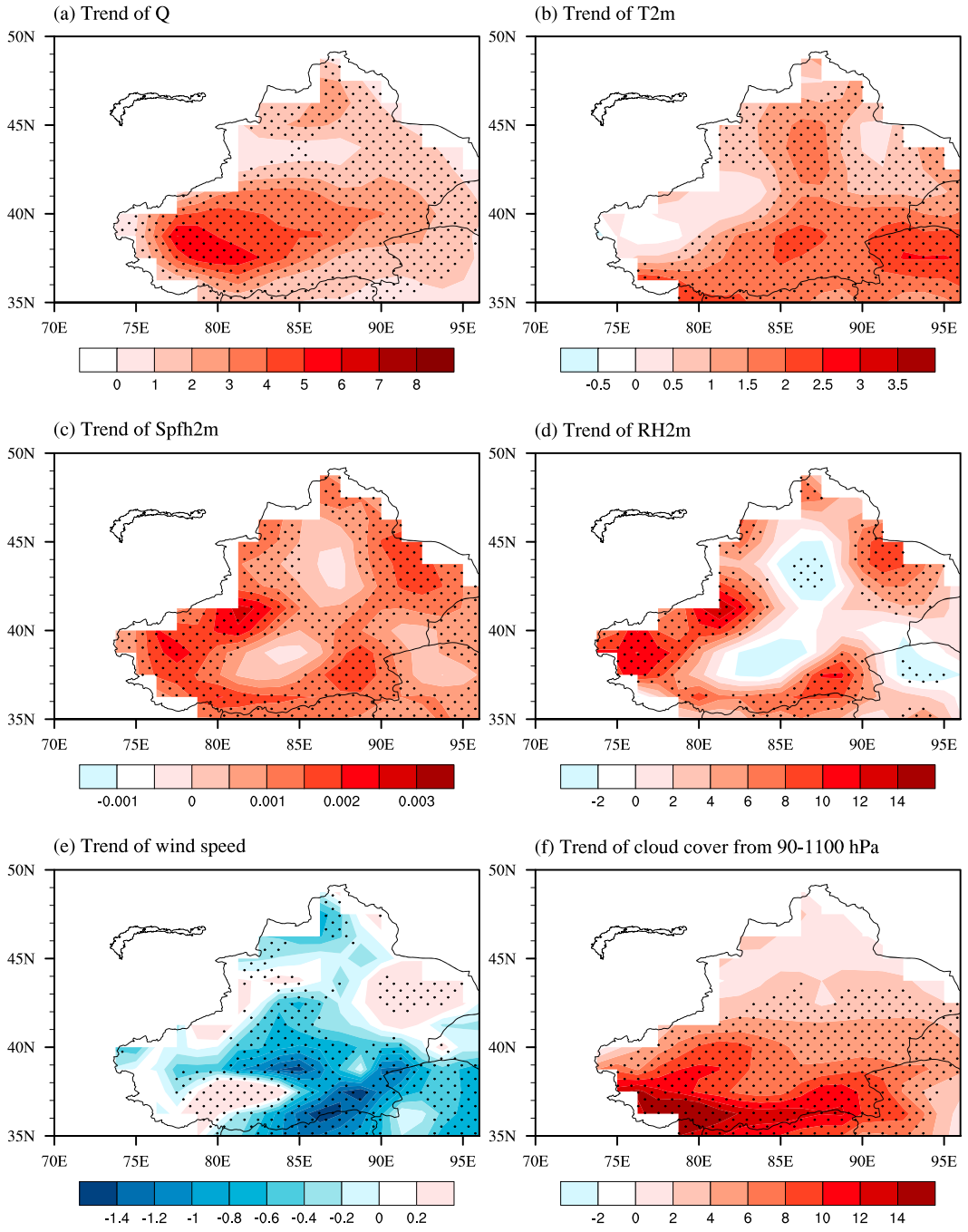

Figure 8. (a) The spatial patterns of long-term trend for (a) vertically integrated precipitable water (*Q*, units: kg m^{-2} 50 yr^{-1}), (b) T2m (units: °C 50 yr^{-1}), (c) near-surface specific humidity (spfh2m, units: kg kg^{-1} 50 yr^{-1}), (d) RH2m (units: % 50 yr^{-1}), (e) near-surface wind speed (units: m s^{-1} 50 yr^{-1}), and (f) the total cloud cover from 90 to 1100 hPa (units: % 50 yr^{-1}). Dotted regions are statistically significant at the 10% level.

multiplied by the horizontal gradient of vertical vorticity ($-\vec{\boldsymbol{V}}_{\boldsymbol{h}}\,\nabla_{\boldsymbol{h}}\cdot\zeta$); ζ is the vertical vorticity) at 500 hPa (Figure 9c). When the ASWJ is located to the south, the vorticity advection over WNW intensifies, inducing the anomalous upward motion ($\omega' \propto \overrightarrow{\left(\boldsymbol{V}_{\boldsymbol{h}}\,\nabla_{\boldsymbol{h}}\cdot\zeta\right)'}$ [*Wei et al.*, 2014]) and increasing the precipitation. The southward shift of ASWJ is related with the increased meridional tropospheric temperature gradient which is dominated by the upper tropospheric cooling over Asia [*Yu et al.*, 2004; *Zhou and Zhang*, 2005; *Zhang and Huang*, 2011; *Zhao et al.*, 2014a].

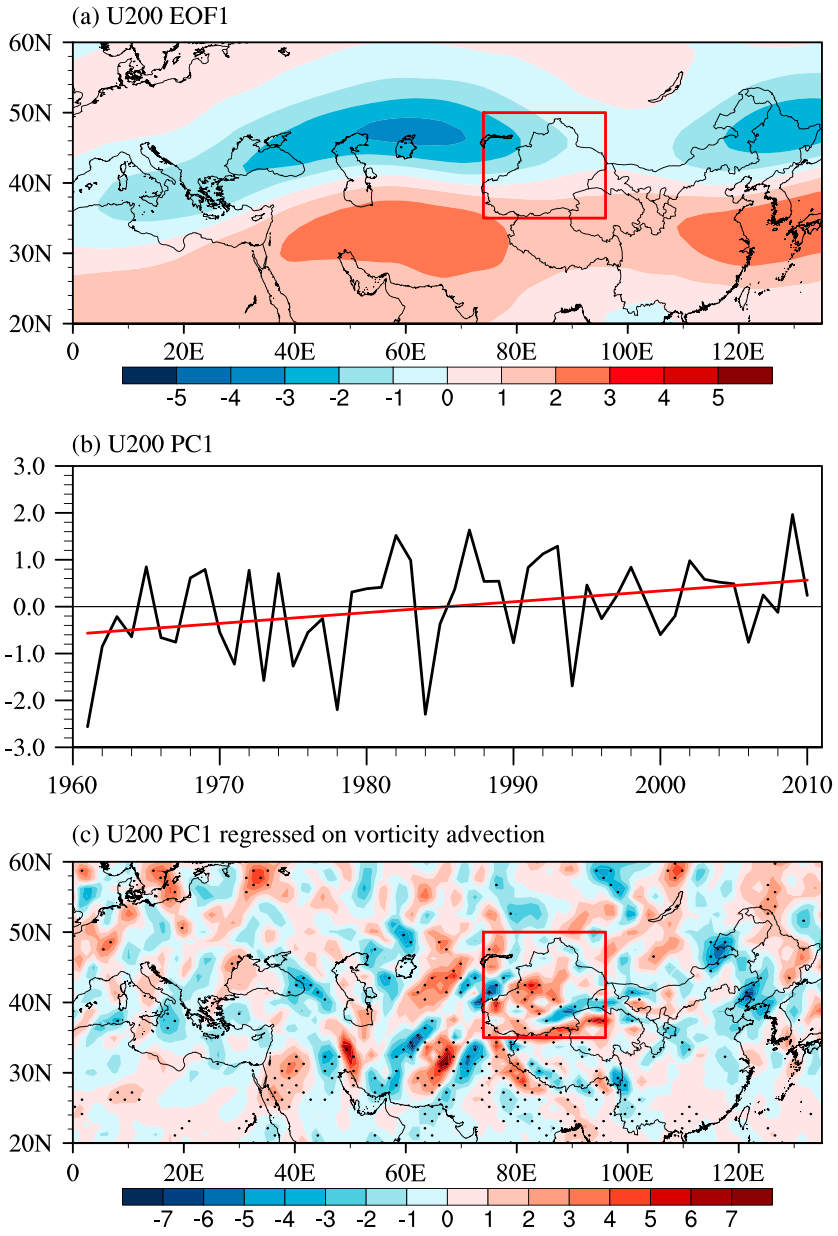

Figure 9. (a) The first leading empirical orthogonal function (EOF) mode of 200 hPa zonal wind over the domain spanning from 20 to 60°N, 0° to 150°E (units: m s^{-1}) and (b) the corresponding principal component (PC) time series (the trend is significant at 10% level). This mode explains 25.1% of the total variance. (c) Anomalies of relative vorticity advection at 500 hPa regressed upon the PC time series in Figure 9b. Units:10^{-10} s^{-1} $year^{-1}$.

4. Summary and Concluding Remarks

Rain gauge observations show an increasing trend of summer precipitation in arid and semiarid NW during 1961–2010, but the mechanisms remain inconclusive. In this study, we conducted the moisture budget analysis to understand the dynamic and physical processes that are responsible for the increasing trend of precipitation. The major processes are depicted in Figure 10. Main findings are summarized below.

1. In arid and semiarid NW, the climatological value of precipitation is nearly equal to that of evaporation. The contributions of wind convergence term ($-<\omega\partial_p q>$) are offset by that of horizontal moisture advection term ($-<\overrightarrow{\boldsymbol{V_h}}\ \nabla_{\boldsymbol{h}}\cdot q>$). Hence, the moisture flux convergence term ($-<\nabla\cdot\overrightarrow{\boldsymbol{V}}q>$), i.e., the sum of wind convergence ($-<\omega\partial_p q>$) and horizontal term ($-<\overrightarrow{\boldsymbol{V_h}}\ \nabla_{\boldsymbol{h}}\cdot q>$), contribute little to the climatological precipitation.

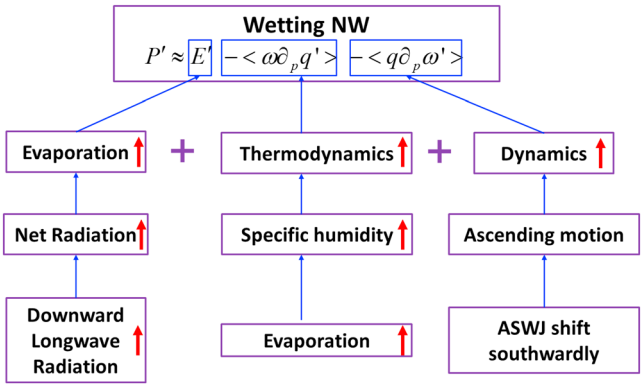

Figure 10. A schematic diagram summarizing the main mechanisms in association with the increasing precipitation in NW from the perspective of moisture budget analysis.

2. More than 50% of the increasing precipitation is balanced by the changes in evaporation. The contribution of moisture flux convergence, which is the sum of negative trend of horizontal moisture advection term and negative trend of wind convergence term, has a significant positive contribution to the wetting trend. The contribution of moisture flux is further separated into thermodynamic component $<\overline{\omega}\ \partial_p q'>$ and dynamic component $-<\omega'\ \partial_p \overline{q}>$. We found that the contribution of thermodynamic component (i.e., changes in specific humidity under fixed atmospheric circulation) is larger than that of dynamic component (i.e., changes in atmospheric circulation under fixed specific humidity). Therefore, the increasing trend of precipitation minus evaporation over NW is dominated by the changes of thermodynamic component, followed by dynamic component.
3. The increasing net radiation, which mainly results from more downward longwave radiation associated with warming atmosphere, favors the process of evaporation. The contribution of thermodynamic component is linked with increased specific humidity which is associated with enhanced evaporation. The dynamic contribution to changes in precipitation refers to the contribution caused by changes in atmospheric circulation. Results show that the anomalous cyclone over central Asia is related to the southward displacement of ASWJ. During 1961–2010, the ASWJ has experienced a significant southward displacement, which intensifies the vorticity advection over NW, thus inducing anomalous upward motion and increasing the precipitation.

Finally, while the moisture budget analysis presented in this study has revealed the dynamic and physical processes that are responsible for the increasing trend of precipitation, we acknowledge that the results based on moisture budget analysis are mainly focused on the immediate causes and mechanisms. It is difficult to completely disentangle the cause-and-effect relationship between the rather complex interactive land-atmosphere system in the local area, such as the coherent linkage between the precipitation increase, wetter soil, and the enhanced evaporation.

In addition, previous studies demonstrated that the southward displacement of ASWJ is affected by the upper tropospheric cooling [*Yu et al*., 2004; *Zhang and Huang*, 2011; *Zhao et al*., 2014a], which is partly induced by the anthropogenic aerosol forcing [*Song et al*., 2014]. *Wang et al*. [2013] also showed the evidence that the southward displacement of ASWJ is influenced by anthropogenic forcing. Meanwhile, natural variability such as Pacific Decadal Oscillation (PDO) and Atlantic Multidecadal Oscillation (AMO) is also suggested to affect the meridional displacement of ASWJ [*Zhu et al*., 2015]. The interdecadal to multidecadal variability have great influence on the regional climate change, and the influences of AMO and PDO on central Asian climate are also noted in previous studies [*Meehl et al*., 2013; *Dong and Dai*, 2015; *Wu et al*, 2016]. The coherent changes of AMO/PDO, ASWJ, and central Asian precipitation, in particular how these processes led to all the local changes presented in this study, deserve further study.

Acknowledgments
This work is jointly supported by R&D Special Fund for Public Welfare Industry (meteorology) (GYHY201506012) and National Natural Science Foundation of China under grants 41330423 and 41420104006. This work was also supported by the Jiangsu Collaborative Innovation Center for Climate Change. The rain gauge data used in the paper are provided by CMDC/CMA and can be accessed from http://data.cma.cn/en after registration and signing an agreement of data sharing. Readers who have difficulties in accessing the data directly from the CMDC website may contact Tianjun Zhou via zhoutj@lasg.iap.ac.cn for personal scientific research and education usage of the portion of the data used in the study.

References

Allen, R. G., L. S. Pereira, D. Raes, and M. Smith (1998), Crop evapotranspiration—Guidelines for computing crop water requirements, in *FAO Irrigation and Drainage Paper*, vol. 56, pp. 29–35, FAO, Rome.

Brutsaert, W. (2006), Indications of increasing land surface evaporation during the second half of the 20th century, *Geophys. Res. Lett.*, *33*, L20403, doi:10.1029/2006GL027532.

Burn, D. H., and N. M. Hesch (2007), Trends in evaporation for the Canadian prairies, *J. Hydrol.*, *336*(1), 61–73, doi:10.1016/j.jhydrol.2006.12.011.

Chattopadhyay, N., and, M. Hulme (1997), Evaporation and potential evapotranspiration in India under conditions of recent and future climate change, *Agric. For. Meteorol.*, *87*(1), 55–73, doi:10.1016/S0168-1923(97)00006-3.

Chen, D. D., and Y. J. Dai (2009), Characteristics and analysis of typical anomalous summer rainfall patterns in northwest China over the last 50 years [in Chinese], *Chin. J. Atmos. Sci.*, *33*(6), 1247–1258, doi:10.3878/j.issn.1006-9895.2009.06.11.

Chen, G., and R. Huang (2012), Excitation mechanisms of the teleconnection patterns affecting the July precipitation in northwest China, *J. Clim.*, *25*(22), 7834–7851, doi:10.1175/JCLI-D-11-00684.1.
Chen, Z., Y. Chen, and B. Li (2013), Quantifying the effects of climate variability and human activities on runoff for Kaidu River basin in arid region of north-west China, *Theor. Appl. Climatol.*, *111*(3–4), 537–545, doi:10.1007/s00704-012-0680-4.
Chou, C., and C. W. Lan (2012), Changes in the annual range of precipitation under global warming, *J. Clim.*, *25*(1), 222–235, doi:10.1175/JCLI-D-11-00097.1.
Chou, C., and J. D. Neelin (2004), Mechanisms of global warming impacts on regional tropical precipitation, *J. Clim.*, *17*(13), 2688–2701, doi:10.1175/1520-0442(2004)017<2688:mogwio>2.0.co;2.
Chou, C., J. C. H. Chiang, C. W. Lan, C. H. Chung, Y. C. Liao, and C. J. Lee (2013), Increase in the range between wet and dry season precipitation, *Nat. Geosci.*, *6*(4), 263–267, doi:10.1038/NGEO1744.
Chou, C., J. D. Neelin, C. A. Chen, and J. Y. Tu (2009), Evaluating the "rich-get-richer" mechanism in tropical precipitation change under global warming, *J. Clim.*, *22*(8), 1982–2005, doi:10.1175/2008JCLI2471.1.
CMA (2014), *China Climate Bulletin for 2013*, p. 15, China Meteorol. Admin., Beijing.
Ding, Q., and B. Wang (2005), Circumglobal teleconnection in the Northern Hemisphere summer, *J. Clim.*, *18*(17), 3483–3505, doi:10.1175/JCLI3473.1.
Ding, Q., B. Wang, J. M. Wallace, and G. Branstator (2011), Tropical-extratropical teleconnections in boreal summer: Observed interannual variability, *J. Clim.*, *24*(7), 1878–1896, doi:10.1175/2011JCLI3621.1.
Dong, B., and A. G. Dai (2015), The influence of the interdecadal Pacific oscillation on temperature and precipitation over the globe, *Clim. Dyn.*, *45*(9–10), 2667–2681, doi:10.1007/s00382-015-2500-x.
Feng, L., and T. Zhou (2012), Water vapor transport for summer precipitation over the Tibetan Plateau: Multi-dataset analysis, *J. Geophys. Res.*, *117*, D20114, doi:10.1029/2011JD017012.
Feng, W., K. L. Wang, and H. Jiang (2004), Influences of westerly wind interannual change on water vapor transport over northwest China summer [in Chinese], *Plateau Meteorol.*, *23*(02), 271–275.
Greve, P., B. Orlowsky, B. Mueller, J. Sheffield, M. Reichstein, and S. I. Seneviratne (2014), Global assessment of trends in wetting and drying over land, *Nat. Geosci.*, *7*(10), 716–721, doi:10.1038/ngeo2247.
Han, X., H. Xue, C. Zhao, and D. R. Lu (2016), The roles of convective and stratiform precipitation in the observed precipitation trends in Northwest China during 1961–2000, *Atmos. Res.*, *169*, 139–146, doi:10.1016/j.atmosres.2015.10.001.
Held, I. M., and B. J. Soden (2006), Robust responses of the hydrological cycle to global warming, *J. Clim.*, *19*(21), 5686–5699, doi:10.1175/JCLI3990.1.
Hong, X., and R. Lu (2016), The meridional displacement of the summer Asian jet, silk road pattern, and tropical SST anomalies, *J. Clim.*, *29*(10), 3753–3766, doi:10.1175/JCLI-D-15-0541.1.
Huang, W., S. Feng, J. Chen, and F. Chen (2015), Physical mechanisms of summer precipitation variations in the Tarim Basin in Northwestern China, *J. Clim.*, *28*(9), 3579–3591, doi:10.1175/JCLI-D-14-00395.1.
Intergovernmental Panel on Climate Change (IPCC) (2013), *Climate Change 2013: The Physical Science Basis: Working Group I Contribution to the Fifth Assessment Report of the Intergovernmental Panel on Climate Change*, edited by T. F. Stocker et al., Cambridge Univ. Press, Cambridge, U. K.
Ji, Z. M., and S. C. Kang (2015), Evaluation of extreme climate events using a regional climate model for China, *Int. J. Climatol.*, *35*(6), 888–902, doi:10.1002/joc.4024.
Jiang, F. Q., R. J. Hu, S. P. Wang, Y. W. Zhang, and L. Tong (2013), Trends of precipitation extremes during 1960–2008 in Xinjiang, the northwest China, *Theor. Appl. Climatol.*, *111*(1–2), 133–148, doi:10.1007/s00704-012-0657-3.
JMA (2013), JRA-55 product users' handbook: 1.25 degree latitude/longitude grid data. [Available at http://jra.kishou.go.jp/JRA-55/index_en.html.]
Kobayashi, S., et al. (2015), The JRA-55 reanalysis: General specifications and basic characteristics, *J. Meteorol. Soc. Jpn.*, *93*(1), 5–48, doi:10.2151/jmsj.2015-001.
Koster, R. D., et al. (2004), Regions of strong coupling between soil moisture and precipitation, *Science*, *305*(5687), 1138–1140, doi:10.1126/science.1100217.
Li, B., Y. Chen, Z. Chen, H. Xiong, and L. Lian (2016), Why does precipitation in northwest China show a significant increasing trend from 1960 to 2010?, *Atmos. Res.*, *167*, 275–284, doi:10.1016/j.atmosres.2015.08.017.
Li, W. L., K. L. Wang, S. M. Fu, and H. Jiang (2008), The interrelationship between regional westerly index and the water vapor budget in northwest China [in Chinese], *J. Glaciol. Geocryol.*, *30*(1), 34–38.
Li, X. S. (2013), Changing characteristics of snowfall in Xinjiang from 1961–2010 [in Chinese], MD thesis.
Lin, R. P., T. Zhou, and Y. Qian (2014), Evaluation of global monsoon precipitation changes based on five reanalysis datasets, *J. Clim.*, *27*(3), 1271–1289, doi:10.1175/JCLI-D-13-00215.1.
Liu, L., R. H. Zhang, and Z. Y. Zuo (2014), Intercomparison of spring soil moisture among multiple reanalysis data sets over eastern China, *J. Geophys. Res. Atmos.*, *119*, 54–64, doi:10.1002/2013JD020940.
Lorenz, D. J., E. T. DeWeaver, and D. J. Vimont (2010), Evaporation change and global warming: The role of net radiation and relative humidity, *J. Geophys. Res.*, *115*, D20118, doi:10.1029/2010JD013949.
Lu, A. G., Y. J. Ding, H. X. Pang, and L. L. Yuan (2005), Impact of global warming on water resource in arid area of northwest China, *J. Mt. Sci.*, *2*(4), 313–318, doi:10.1007/BF02918404.
Lu, E., et al. (2014), Changes of summer precipitation in China: The dominance of frequency and intensity and linkage with changes in moisture and air temperature, *J. Geophys. Res. Atmos.*, *119*, 12,575–12,587, doi:10.1002/2014JD022456.
Ma, S., and T. Zhou (2015), Precipitation changes in wet and dry seasons over the 20th century simulated by two versions of the FGOALS model, *Adv. Atmos. Sci.*, *32*(6), 839–854, doi:10.1007/s00376-014-4136-x.
Ma, S., T. Zhou, A. Dai, and Z. Y. Han (2015), Observed changes in the distributions of daily precipitation frequency and amount over China from 1960 to 2013, *J. Clim.*, *28*(17), 6960–6978, doi:10.1175/JCLI-D-15-0011.1.
Meehl, G. A., A. X. Hu, J. M. Arblaster, J. Fasullo, and K. E. Trenberth (2013), Externally forced and internally generated decadal climate variability associated with the interdecadal Pacific oscillation, *J. Clim.*, *26*(18), 7298–7310, doi:10.1175/JCLI-D-12-00548.1.
Qian, W. H., J. L. Fu, and Z. W. Yan (2007), Decrease of light rain events in summer associated with a warming environment in China during 1961–2005, *Geophys. Res. Lett.*, *34*, L11705, doi:10.1029/2007GL029631.
Qian, Z. A., T. W. Wu, S. Lu, and Y. Jiao (1998), Numerical simulation of northwest China arid climate formation—Effects of the Qinghai-Xizang plateau terrain and circulation field [in Chinese], *Chin. J. Atmos. Sci.*, *22*(5), 753–762.
Qian, Z. A., T. W. Wu, and X. Y. Liang (2001a), Feature of mean vertical circulation over the Qinghai-Xizang plateau and its neighborhood [in Chinese], *Chin. J. Atmos. Sci.*, *25*(4), 444–454.

Qian, Z. A., T. W. Wu, M. H. Song, X. B. Ma, Y. Cai, and X. Y. Liang (2001b), Arid disaster and advances in arid climate researched over northwest China [in Chinese], *Adv. Earth Sci.*, *6*(01), 28–38.
Ren, G. Y., J. Guo, Z. M. Xu, Z. Y. Chu, L. Zhang, X. K. Zou, Q. X. Li, and X. N. Liu (2005), Climate changes of China's mainland over the past half century [in Chinese], *Acta Meteorol. Sin.*, *63*(6), 942–956.
Ren, G. Y., Y. J. Yuan, Y. J. Liu, Y. Y. Ren, T. Wang, and X. Y. Ren (2016), Changes in precipitation over northwest China [in Chinese], *Arid Zone Res.*, *33*(1), 1–19, doi:10.13866/j.azr.2016.01.01.
Seager, R., N. Naik, and G. A. Vecchi (2010), Thermodynamic and dynamic mechanisms for large-scale changes in the hydrological cycle in response to global warming, *J. Clim.*, *23*(17), 4651–4668, doi:10.1175/2010JCLI3655.1.
Shangguan, D. H., S. Liu, Y. Ding, L. F. Ding, J. L. Xu, and L. Jing (2009), Glacier changes during the last forty years in the Tarim Interior River basin, northwest China, *Prog. Nat. Sci.*, *19*(6), 727–732, doi:10.1016/j.pnsc.2008.11.002.
Shi, Y., Y. Shen, E. Kang, D. Li, Y. Ding, G. Zhang, and R. Hu (2007), Recent and future climate change in northwest China, *Clim. Change*, *80*(3–4), 379–393, doi:10.1007/s10584-006-9121-7.
Song, F. F. T., J. Zhou, and Y. Qian (2014), Responses of East Asian summer monsoon to natural and anthropogenic forcings in the 17 latest CMIP5 models, *Geophys. Res. Lett.*, *41*, 596–603, doi:10.1002/2013GL058705.
Song, L. C., and C. J. Zhang (2003), Changing features of precipitation over northwest China during the 20th century, *J. Glaciol. Geocryol.*, *25*(2), 143–148.
Su, T., T. C. Feng, and G. L. Feng (2015), Evaporation variability under climate warming in five reanalyses and its association with pan evaporation over China, *J. Geophys. Res. Atmos.*, *120*, 8080–8098, doi:10.1002/2014JD023040.
Sun, J., H. Wang, W. Yuan, and H. P. Chen (2010), Spatial-temporal features of intense snowfall events in China and their possible change, *J. Geophys. Res.*, *115*, D16110, doi:10.1029/2009JD013541.
Trenberth, K. E., and C. J. Guillemot (1995), Evaluation of the global atmospheric moisture budget as seen from analyses, *J. Clim.*, *8*(9), 2255–2272, doi:10.1175/1520-0442(1995)008<2255:EOTGAM>2.0.CO;2.
Wang, A. H., D. P. Lettenmaier, and J. Sheffield (2011), Soil moisture drought in China, 1950–2006, *J. Clim.*, *24*(13), 3257–3271, doi:10.1175/2011JCLI3733.1.
Wang, P., Z. Q. Li, and W. Y. Gao (2011), Rapid shrinking of glaciers in the middle Qilian Mountain region of northwest China during the last ~50 years, *J. Earth Sci.*, *22*(4), 539–548, doi:10.1007/s12583-011-0195-4.
Wang, T., H. J. Wang, O. H. Otterå, Y. Q. Gao, L. L. Suo, T. Furevik, and L. Yu (2013), Anthropogenic agent implicated as a prime driver of shift in precipitation in eastern China in the late 1970s, *Atmos. Chem. Phys.*, *13*(24), 12433–12450, doi:10.5194/acp-13-12433-2013.
Wei, W., R. Zhang, W. Min, X. Y. Rong, and T. Li (2014), Impact of Indian summer monsoon on the south Asian high and its influence on summer rainfall over China, *Clim. Dyn.*, *43*, 1257–1269, doi:10.1007/s00382-013-1938-y.
Wei, W., R. Zhang, M. Wen, and S. Yang (2017), Relationship between the Asian westerly jet stream and summer rainfall over central Asia and north China: Roles of the Indian monsoon and the south Asian high, *J. Clim.*, *30*(2), 537–552, doi:10.1175/JCLI-D-15-0814.1.
Wu, B., T. Zhou, and T. Li (2016), Impacts of the Pacific–Japan and Circumglobal teleconnection patterns on the interdecadal variability of the East Asian Summer Monsoon, *J. Clim.*, *29*(9), 3253–3271, doi:10.1175/JCLI-D-15-0105.1.
Wu, J., and X. J. Gao (2013), A gridded daily observation dataset over China region and comparison with the other datasets [in Chinese], *Chin. J. Geophys.*, *56*(4), 1102–1111, doi:10.6038/cjg20130406.
Wu, T. W., and Z. A. Qian (1996), The comparative analyses of differences between vertical circulation on north side of Tibetan Plateau in wet and dry summer and thermal effects of the plateau [in Chinese], *Acta Meteorol. Sin.*, *54*(6), 558–568.
Yao, T., Y. Wang, S. Liu, J. C. Pu, Y. P. Shen, and A. X. Lu (2004), Recent glacial retreat in high Asia in China and its impact on water resource in northwest China [J], *Sci. China Ser. D Earth Sci.*, *47*(12), 1065–1075, doi:10.1360/03yd0256.
Yu, R., B. Wang, and T. Zhou (2004), Tropospheric cooling and summer monsoon weakening trend over East Asia, *Geophys. Res. Lett.*, *31*, L22212, doi:10.1029/2004GL021270.
Zhai, P. M., F. M. and Ren, Q. Zhang (1999), Detection of trend in China's precipitation extremes [in Chinese], *Acta Meteorol. Sin.*, *57*(2), 208–215.
Zhang, Y. C., and D. Q. Huang (2011), Has the East Asian westerly jet experienced a poleward displacement in recent decades? *Adv. Atmos. Sci.*, *28*(6), 1259–1265, doi:10.1007/s00376-011-9185-9.
Zhao, C., S. Yao, J. Liu, and J. Wang (2014), The spatial distribution of precipitation in northwest China, *J. Electric. Comput. Eng.*, *2014*(1), 1–5, doi:10.1155/2014/514291.
Zhao, Y., A. Huang, Y. Zhou, D. Q. Huang, Q. Yang, Y. F. Ma, M. Li, and G. Wei (2014a), Impact of the middle and upper tropospheric cooling over central Asia on the summer rainfall in the Tarim Basin, China, *J. Clim.*, *27*(12), 4721–4732, doi:10.1175/JCLI-D-13-00456.1.
Zhao, Y., M. Wang, A. Huang, H. Li, W. Huo, and Q. Yang (2014b), Relationships between the west Asian subtropical westerly jet and summer precipitation in northern Xinjiang, *Theor. Appl. Climatol.*, *116*(3–4), 403–411, doi:10.1007/s00704-013-0948-3.
Zhou, B. T., Y. Xu, J. Wu, S. Y. Dong, and Y. Shi (2015), Changes in temperature and precipitation extreme indices over China: Analysis of a high-resolution grid dataset, *Int. J. Climatol.*, *36*, 1051–1066, doi:10.1002/joc.4400.
Zhou, L. T., and R. H. Huang (2010), Interdecadal variability of summer rainfall in northwest China and its possible causes, *Int. J. Climatol.*, *30*(4), 549–557, doi:10.1002/joc.1923.
Zhou, S. W., and R. H. Zhang (2005), Decadal variations of temperature and geopotential height over the Tibetan Plateau and their relations with Tibet ozone depletion, *Geophys. Res. Lett.*, *32*, L18705, doi:10.1029/2005GL023496.
Zhu, Y., H. J. Wang, J. H. Ma, T. Wang, and J. Q. Sun (2015), Contribution of the phase transition of Pacific decadal oscillation to the late 1990s' shift in East China summer rainfall, *J. Geophys. Res. Atmos.*, *120*, 8817–8827, doi:10.1002/2015JD023545.